New insights into structural disorder in human respiratory syncytial virus phosphoprotein and implications for binding of protein partners

Nelson Pereira, Christophe Cardone, Safa Lassoued, Marie Galloux, Jenna Fix, Nadine Assrir, Ewen Lescop, Francois Bontems, Jean Francois Eleouet, Christina Sizun

THE JOURNAL OF BIOLOGICAL CHEMISTRY VOL. 292, NO. 6, pp. 2120–2131, February 10, 2017

New Insights into Structural Disorder in Human Respiratory Syncytial Virus Phosphoprotein and Implications for Binding of Protein Partners*

Received for publication, November 2, 2016, and in revised form, December 21, 2016 Published, JBC Papers in Press, December 28, 2016, DOI 10.1074/jbc.M116.765958

Nelson Pereira[‡1], **Christophe Cardone**[‡1], **Safa Lassoued**[‡1], **Marie Galloux**[§], **Jenna Fix**[§], **Nadine Assrir**[‡], **Ewen Lescop**[‡], **François Bontems**[‡], **Jean-François Eléouët**[§], **and Christina Sizun**[‡2]

From the [‡]*Institut de Chimie des Substances Naturelles, UPR2301, Centre National de la Recherche Scientifique, Université Paris Saclay, 91190 Gif-sur-Yvette and the* [§]*Unité de Virologie et Immunologie Moléculaires, UR892, Institut National de la Recherche Agronomique, 78350 Jouy-en-Josas, France*

Edited by Charles E. Samuel

Phosphoprotein is the main cofactor of the viral RNA polymerase of *Mononegavirales*. It is involved in multiple interactions that are essential for the polymerase function. Most prominently it positions the polymerase complex onto the nucleocapsid, but also acts as a chaperone for the nucleoprotein. *Mononegavirales* phosphoproteins lack sequence conservation, but contain all large disordered regions. We show here that N- and C-terminal intrinsically disordered regions account for 80% of the phosphoprotein of the respiratory syncytial virus. But these regions display marked dynamic heterogeneity. Whereas almost stable helices are formed C terminally to the oligomerization domain, extremely transient helices are present in the N-terminal region. They all mediate internal long-range contacts in this non-globular protein. Transient secondary elements together with fully disordered regions also provide protein binding sites recognized by the respiratory syncytial virus nucleoprotein and compatible with weak interactions required for the processivity of the polymerase.

Human respiratory syncytial virus (hRSV),[3] a member of the family *Pneumoviridae* (1) and order *Mononegavirales* (MNV), is the main viral cause of lower respiratory tract illness worldwide, and the main agent responsible for bronchiolitis and pneumonia in infants (2). All children have been infected by the age of two, requiring hospitalization in ~5% cases (3). Elderly and immunocompromised adults are also at increased risk. No efficient treatment is presently available for hRSV (4), and vaccination is challenging due to complex immunogenicity (5). The search for hRSV antiviral drugs directed toward specific viral functions is therefore still ongoing (6).

The hRSV RNA-dependent RNA complex (RdRp) constitutes a virus-specific target with specific protein-protein interactions that have not all been investigated in detail (7). It uses the nonsegmented single-stranded negative sense RNA genome of hRSV as a template. In infected cells, the viral RdRp is found in specific inclusion bodies (8), which have been shown to be transcription and replication centers for other *Mononegavirales*, *e.g.* rabies (9) and vesicular stomatitis viruses (10). The apo RdRp complex is composed *a minima* of the large catalytic subunit (L) and its essential cofactor, the phosphoprotein (P) (11, 12). The P protein plays a central role in the RdRp by interacting with all main RdRp components. During transcription and replication it tethers the L protein to the nucleocapsid (NC), consisting of the genomic RNA packaged by the nucleoprotein (N), by direct interaction with N (13–16). hRSV P also binds to the transcription antitermination factor M2-1 (17–19). Phosphorylation of P has been proposed to regulate these interactions, although it is not essential for replication (20–22). P also acts as a chaperone for neo-synthesized N by forming an N^0·P complex that preserves N in a monomeric and RNA-free state (23). We have shown previously that formation of hRSV NC·P and N^0·P complexes proceeds via two distinct binding sites on P (14, 24).

Bioinformatic and biochemical investigations have established that hRSV P is tetrameric and contains large disordered N- and C-terminal regions (25–27). Fragment Y* (Table 1) was described as a minimal oligomerization domain (OD) with predicted helical coiled-coil structure (28). However, a clear picture of the overall structure of P is still lacking, mainly because of its structural disorder. Our aim was to get a deeper insight into the structural plasticity of P and to explore the role of transiently ordered regions for interactions with hRSV RdRp proteins, here with N, by using NMR spectroscopy.

* This work was supported by Agence Nationale de la Recherche Grants ANR-11-BSV8-024-02 and ANR-13-ISV3-0007-04 and doctoral fellowships from Institut de Chimie des Substances Naturelles (to N. P.) and Région Ile-de-France DIM Malinf (to S. L. and C. C.). The authors declare that they have no conflicts of interest with the contents of this article.

Data were deposited at the Biological Magnetic Resonance Bank with accession numbers 26902, 26903, 26904, 26905, and 26906 for P_{ND}, $P_{\Delta OD}$, P_{ND+OD}, P_{FL}-S23C, and P_{CD}, respectively.

[1] These authors contributed equally to the results of this work.

[2] To whom correspondence should be addressed: ICSN, CNRS, 1 Avenue de la Terrasse, 91190 Gif-sur-Yvette, France. Tel.: 33-169823764; Fax: 33-169823784; E-mail: christina.sizun@cnrs.fr.

[3] The abbreviations used are: hRSV, human respiratory syncytial virus; CSP, chemical shift perturbation; HSQC, heteronuclear single quantum spectroscopy; IDP/R, intrinsically disordered protein/region; MPV, *Metapneumovirus*; N, nucleoprotein; NCBD, nucleocapsid binding domain; NC, nucleocapsid; OD, oligomerization domain; P, phosphoprotein; RdRp, RNA-dependent RNA polymerase; RSV, respiratory syncytial virus; SSP, secondary structure propensity; PRE, paramagnetic relaxation enhancement; hMPV, human *Metapneumovirus*; IAP, 3-(2-iodoacetamido)-PROXYL.

Results

Extent of Intrinsically Disordered Regions in hRSV Phosphoprotein—To probe the structural organization of hRSV phosphoprotein at the single residue level by NMR, we first used full-length P protein (P_{FL}). The two-dimensional ^{1}H-^{15}N HSQC spectrum of P_{FL} exhibits sharp amide signals with narrow ^{1}H chemical shift dispersion in the 7.5–8.5 ppm range (Fig. 1). This is the signature of intrinsically disordered proteins (IDPs) and regions (IDRs) (29). Experimental conditions were adjusted for the detection of IDP amide protons, low temperature (288 K) and acidic pH (6.5), to reduce the contribution of water exchange to line widths. Only 60% (140 of 229) of expected P_{FL} amide signals were observed. 40% of amide signals were too broad to be detected and correspond to protein regions undergoing dynamic processes and conformational exchange at the μs-ms time scale. They comprise the OD (fragment Y*, ~40 residues), but also extensive additional regions (~50 residues).

Due to the structural heterogeneity of P, we resorted to protein fragments to delineate domains. Several fragments had been produced before (13, 24, 25, 30). Constructs are detailed in Table 1. In particular, P_{ND+OD} and P_{OD+CD} correspond to the N- and C-terminal domains with OD. P_{ND} and P_{CD} are their counterparts without OD. The ^{1}H-^{15}N HSQC spectra of P fragments exhibit sharp lines and narrow ^{1}H chemical shift dispersion, similarly to P_{FL} (Fig. 1). All signals superimpose well, showing that the fragments are representative of the corresponding domains in P_{FL}. For instance, overlay of P_{ND+OD} and P_{OD+CD} spectra reproduces the spectrum of P_{FL} (Fig. 1). Comparison of P_{ND} and P_{ND+OD} indicates that the OD signals are missing for P_{ND+OD}. Remarkably, fragment P_{CD} displays more signals than P_{OD+CD}, revealing that the C-terminal domain of P contains residues that are not completely disordered when attached to the OD (Fig. 1).

Sequential assignment of backbone chemical shifts was carried out separately for all fragments. The signals of the 120 N-terminal residues and 40 C-terminal residues could be observed for all constructs, including P_{FL}, indicating that they form two independent N- and C-terminal IDRs in P. The signals of the Asp^{125}-Thr^{160} region, equivalent to fragment Y* (Table 1), were missing for all constructs containing the OD. Residues Ser^{161}-Glu^{204} were also missing in the spectra of P_{OD+CD} and P_{FL}, but were present in the spectrum of P_{CD}.

Determination of Transient Secondary Structure Elements in hRSV Phosphoprotein—On closer inspection, many NMR signals display local heterogeneity in intensity and line width. Taking advantage of the sensitivity of ^{13}C backbone and $^{1}H\alpha$ chemical shifts to protein dihedral angles, we determined residue-specific secondary structure propensities (SSPs) in P_{ND}, P_{ND+OD}, P_{CD}, $P_{\Delta OD}$, and P_{FL}, using Talos+ (31) (Fig. 2*A*). Outside the Ser^{161}-Glu^{204} region no significant secondary structure was detected. This confirms that the N and C termini of P are fully disordered. Still, weak α-helical propensity is observed in the N-terminal IDR for residues Asp^{12}-Ile^{24} and Phe^{98}-Lys^{103}. The latter define two transient helices α_{N1} and α_{N2} (Fig. 2*B*).

In contrast, residues Leu^{173}-Lys^{205}, which can only be observed in P fragments devoid of the OD, display high α-helical propensity and define two helices, α_{C1} (Leu^{173}-Met^{187}) and α_{C2} (Asn^{189}-Lys^{205}), with up to 70 and 95% propensity, respectively (Fig. 2, *A* and *B*). Because SSPs depend on the model used to extract them, we also extracted SSPs with δ2D (32). We obtained lower α-helical propensities than with Talos+ (up to 20% for α_{C1} and 70% for α_{C2}), indicating that these helices are also transient, with α_{C2} being almost stable. The $\alpha_{C1/2}$ region does not induce oligomerization on its own, because $P_{\Delta OD}$ and P_{CD} display the same line widths as P_{ND} (Fig. 1). α_{C1} and α_{C2} thus form a second C-terminal IDR with high α-helical propensity, in addition to the fully disordered C terminus. This domain likely accounts for the thermal transition observed in P at physiological temperature (27), indicating that these helices do not tightly associate in the P tetramer. Signal broadening of $\alpha_{C1/2}$ in tetrameric P fragments may be explained by the increased molecular size, which affects overall dynamics in solution, or by interactions between these transient helices and possibly with the OD.

Investigation of the Dynamics of hRSV Phosphoprotein by ^{15}N Nuclear Relaxation—We measured ^{15}N relaxation parameters for a tetrameric (P_{ND+OD}) and three monomeric (P_{ND}, P_{CD}, and $P_{\Delta OD}$) fragments of P (Fig. 2*C*) to analyze the dynamic behavior of the different regions of P. P IDRs display overall homogeneous, negative or near zero heteronuclear ^{1}H-^{15}N nuclear Overhauser effects (NOEs), indicative of large amplitude backbone fluctuations on a ps-ns time scale. The $\alpha_{C1/2}$ region displays higher NOE values (0–0.5), suggesting that it is more ordered. This is also the case for the transient α_{N1} helix. ^{15}N transverse relaxation rates (R_2) are more heterogeneous along the sequence of P, but consistent among P fragments. R_2 values are much higher for regions with α-helical SSP as compared with completely random regions, denoting differential tumbling in solution and conformational exchange between disordered and ordered conformational states, on a μs-ms time scale. A fifth region (Asn^{78}-Ser^{86}) without clear SSP displays similar behavior (Fig. 2*C*), suggesting that exchange broadening also arises from internal interactions. ^{15}N longitudinal relaxation rates (R_1), which are not sensitive to exchange, are nearly uniform along the sequence of P, but underline the structural singularity of α_{C1}. Relaxation parameters of P IDRs are globally independent of the length of the fragments, suggesting that their motions are not significantly restricted and that they are not stably associated with any part of the protein.

Detection of Long-range Contacts in hRSV P by Paramagnetic Relaxation Enhancement—Next, we used paramagnetic relaxation enhancement (PRE) to investigate the spatial organization of P. Line broadening due to PRE in a ~15 Å radius around a paramagnetic spin label can be used to measure long-range distances by NMR in globular proteins, but also to probe long-range contacts in IDPs (33, 34). The sequence of P_{FL} does not contain any cysteine. We therefore introduced cysteines by mutating individual residues distributed along the sequence of P_{FL} and labeled them with IAP free radical (35). The $\alpha_{C1/2}$ region remained undetectable in the ^{1}H-^{15}N HSQC spectra of all Cys mutants in their diamagnetic state, similarly to wild type P_{FL}. We therefore concluded that the mutations did not impact P oligomerization. Hence PREs could only be measured outside the OD and $\alpha_{C1/2}$ region.

The PRE profiles (Fig. 3) are all rather broad and consistent with diffuse contacts mediated by large highly flexible regions. Gradually decreasing PREs are observed for up to 40 residues on each side of a spin label in fully disordered regions of P (positions 23, 99, and 237). Moreover all spin labels, except at position 237, induced PREs in more distal regions. Strikingly,

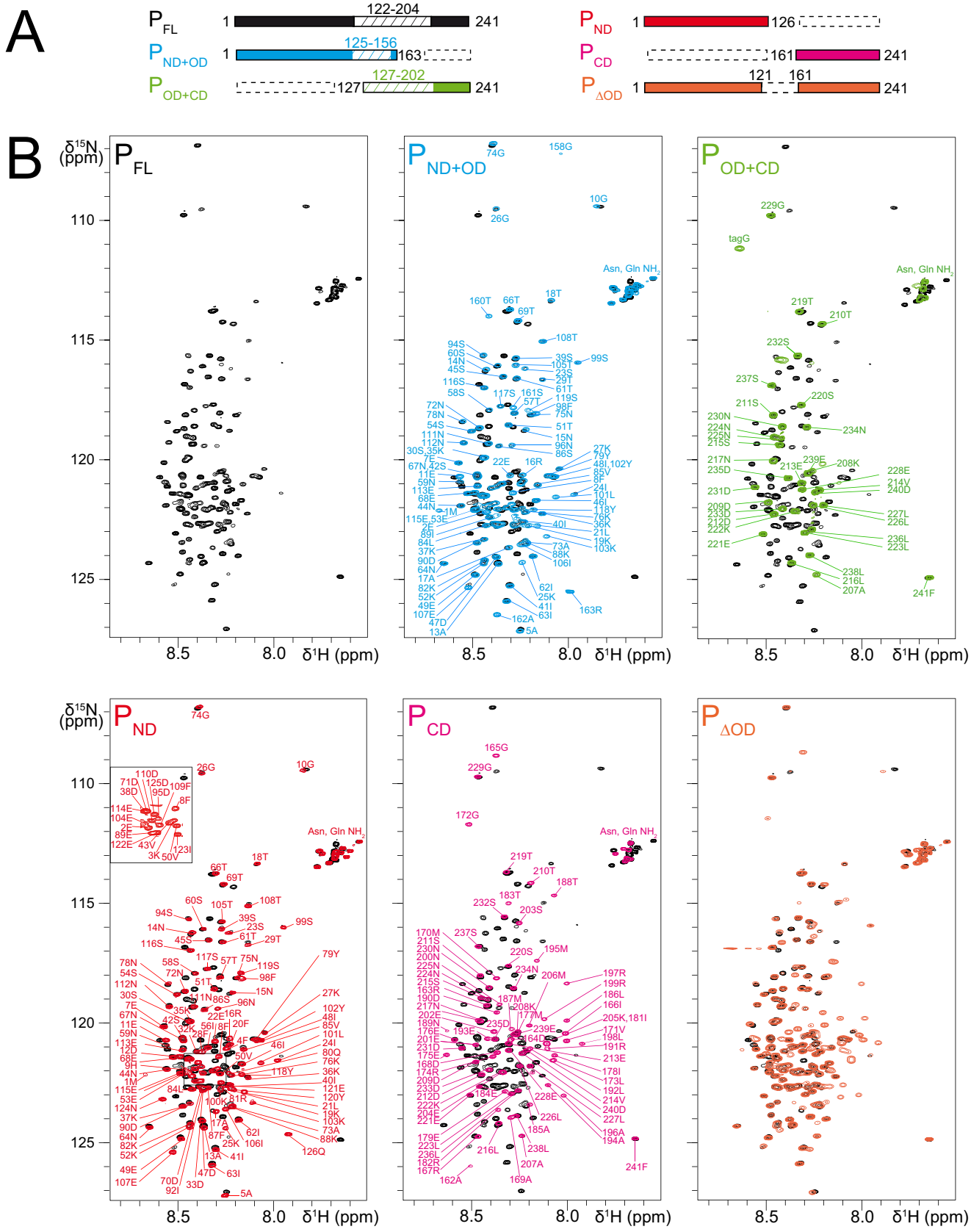

TABLE 1
Definition of hRSV phosphoprotein fragments

Designation of P fragments	Boundaries
P_{FL}	M1-F241
P_{ND+OD}	M1-R163
P_{ND}	M1-Q126
P_{OD+CD}	T127-F241
P_{CD}	S161-F241
$P_{\Delta OD}$	M1-E121+S161-F241
$P_{161-229}$	S161-G229
P_{40}	M1-I40
Fragment X (41)	E104-R163
Fragment Y* (28)	S119-T160

stronger PREs were measured in regions with transient structural elements and in the Asn^{78}-Ser^{86} region, identified by ^{15}N relaxation measurements. Long-range contacts were detected within the N-terminal IDR of P using the S23C and S99C mutants, but also between this region and the OD, using the S143C and S156C mutants, and even the C-terminal α-helical IDR using E179C and E193C. Only the C terminus does not appear to be involved in any specific contact, because strong PREs are only observed for proximal spin labels. The absence of PREs between the C- and N-terminal IDRs moreover provides evidence for a parallel organization of the hRSV P tetramer.

Interactions of hRSV P with Nucleocapsid Analogs—Because transiently structured regions of IDPs are potential molecular recognition elements (36, 37), we carried out NMR interaction experiments to investigate the impact of transient structures within P on hRSV nucleoprotein binding. We first tested N in the form of N-RNA rings, which mimic the hRSV nucleocapsid (38). As the nucleocapsid binding domain of P (P_{NCBD}) had been assigned to its 9 C-terminal residues (13), we worked with ^{15}N-labeled P_{CD} instead of P_{FL}. In the presence of N-RNA rings, the signals of the eight last residues are completely broadened out in the ^{1}H-^{15}N HSQC spectrum of P_{CD} (Fig. 4, *A* and *B*), confirming that they are involved in P binding to the NC. An overall 15% intensity loss seems to arise from increased viscosity, as assessed by a control experiment with excess BSA (Fig. 4*B*).

Direct observation of N-bound P residues by ^{1}H-^{15}N HSQC could not be achieved due to the large size of N-RNA rings. We therefore proceeded with the monomeric N-terminal domain of N (N_{NTD}), which was shown to be relevant for NC·P binding (14, 39). By titrating N_{NTD} into ^{15}N-P_{CD}, linear chemical shift perturbations (CSPs) were observed for P_{NCBD} (*e.g.* Asn^{234} and Ser^{237} in Fig. 4*C*). A titration end point was reached with 5 eq of N_{NTD} (Fig. 4*C*). By fitting the CSP data with a two-site fast exchange model, a K_d of 25–50 μM was determined, in agreement with a K_d of 30 μM previously determined for the N_{NTD}·P_{CD} complex by isothermal titration calorimetry (39).

Notably, CSPs and line broadening occurred concomitantly, pointing to moderately fast exchange between free and N_{NTD}-bound P. However, at the titration end point lines are broader than expected for a 35-kDa complex (Fig. 4*C*). Surprisingly, no signal was recovered for the very C-terminal Phe^{241} residue, which in X-ray structures appears to be the main structural determinant for NC·P complex formation, by tightly inserting into a hydrophobic pocket at the surface of N_{NTD} (39). Our results thus suggest the possibility of additional binding modes corresponding to weaker interactions. Indeed, the large line broadening observed for α_{C1} (Fig. 4*D*) would be in favor of a secondary binding site on α_{C1}. This effect is also observed with the $P_{161-229}$ fragment deleted of P_{NCBD}, although attenuated (Fig. 4*D*), suggesting that binding to α_{C1} could be promoted by binding to P_{NCBD}.

Investigation of the hRSV N^0·P Binding Mode—In a last part we investigated the N^0·P binding mode by using N^{mono}, a monomeric N mutant impaired for RNA binding (24). N^{mono} leads to line broadening at the α_{N1} site in P_{ND+OD} (Fig. 4, *E* and *F*), in agreement with previous results that showed that the N-terminal P_{40} peptide was able to pull down N^{mono} (24). NMR interaction experiments with N^{mono} and P_{FL} show that N^{mono} is competent for both NC·P and N^0·P binding modes, via P_{NCBD} and α_{N1}, respectively (Fig. 4*F*). Because both sites in P_{FL} can be occupied with only 1 eq of N^{mono}, either none of the complexes is very tight or the two sites are not mutually exclusive.

Unexpectedly, a third region, α_{N2}, was perturbed (Fig. 4, *E* and *F*). As previous experiments with the P_{60-126} fragment showed that this region does not bind to N^{mono} (24), line broadening of α_{N2} signals would not be explained by direct binding to N. However, we showed by PRE that α_{N2} transiently associates with α_{N1}. Formation of an N^0·α_{N1} complex could displace the equilibrium between free and α_{N1}-bound α_{N2}.

As a control, we performed additional interaction experiments with ^{15}N-labeled N-terminal P fragments and N_{NTD}. Surprisingly, we observed perturbations (Fig. 5, *A* and *B*). However, the intensity ratio patterns are different from N^{mono}. N^{mono} perturbed a large region (Met^{1}-Ser^{30}), whereas N_{NTD} affects only a few residues around Lys^{25} (Figs. 4*F* and 5*B*), suggesting a difference in binding. We carried out complementary experiments by measuring spectra of ^{15}N-N_{NTD} in the presence of P_{40}. Line broadening was induced in different N_{NTD} regions (Fig. 5, *C* and *D*) delineating a contiguous surface on N (Fig. 5*E*). This surface is on the inside of the nucleocapsid as opposed to the binding site of the C terminus of P in the NC·P complex (Fig. 5*E*). It partly overlaps with the interaction surface of the N-terminal arm of the adjacent protomer in N-RNA rings, but is shifted with respect to the interaction surface recently published for the human *Metapneumovirus* (hMPV) N^0·P complex, where the N-terminal P_{1-28} peptide obstructs the binding sites of the N- and most prominently C-terminal arms of adjacent N protomers (40).

FIGURE 1. **^{1}H-^{15}N HSQC spectra of ^{15}N-labeled RSV phosphoprotein.** *A*, schematic representation of the boundaries of RSV P and P fragments measured by NMR. Deleted regions are symbolized by *boxes in broken line*. *Hatched* areas indicate protein regions with missing amide assignments. *B*, ^{1}H-^{15}N HSQC spectra of P_{FL}, P_{ND+OD}, P_{OD+CD}, P_{ND}, P_{CD}, and $P_{\Delta OD}$ were acquired under identical experimental conditions (50–100 μM concentration, 288 K temperature, 14.1 T magnetic field). A different color was used for each construct to plot contours and show assignments, with full-length P (P_{FL}) in *black*. For all deletion mutants, the spectrum is superimposed onto that of P_{FL} for comparison. Amide resonance assignments are indicated for P_{ND+OD}, P_{OD+CD}, P_{ND}, and P_{CD} (residue number and amino acid type in single-letter code). Asn and Gln NH_2 side chain signals are not individually assigned. For P_{ND} the *inset* shows assignments of the crowded central region of the spectrum.

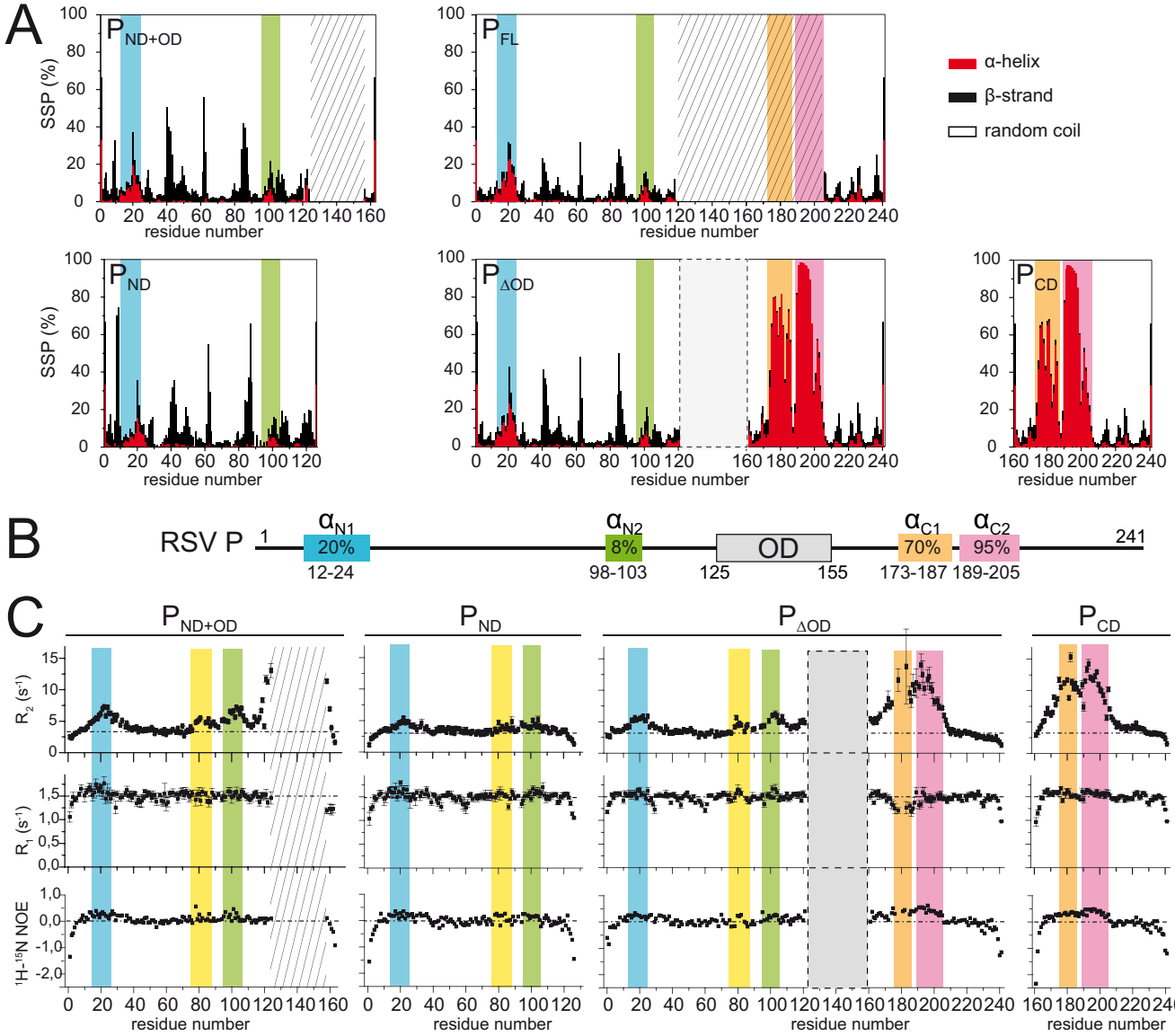

FIGURE 2. **Characterization of structural heterogeneity in hRSV phosphoprotein by backbone chemical shift analysis and ^{15}N relaxation.** *A,* stack plots represent secondary structure propensities (α-helix, β-strand, random coil) of P constructs determined from $^{1}H_{N}$, ^{15}N, $^{1}H\alpha$, $^{13}C'$, $^{13}C\alpha$, and $^{13}C\beta$ chemical shift analysis with Talos+ (31). Notable regions are highlighted by background colors. *Hatched* areas indicate protein regions with missing amide signal. *B,* structural organization of hRSV P as determined from *A*. Transient α-helices are represented as *boxes* with the same color code as in *A*. Maximal α-helical propensity indicated inside. *C,* ^{15}N R_1 and R_2 relaxation rates and heteronuclear ^{1}H-^{15}N NOEs were measured for four P fragments. *Error bars* are S.D. produced by covariance matrix analysis. *Dotted horizontal lines* indicate mean values taking only disordered residues into account. The location of transient α-helices is indicated with the same color code as in *B*. An additional region with dynamics different from IDRs, but not identified in *A*, is highlighted in *yellow*. The hatched area corresponds to the OD. The *box in broken line* indicates the deleted sequence in $P_{\Delta OD}$.

Discussion

Domain Organization in hRSV P—hRSV phosphoprotein is characterized by extensive structural disorder that hampers high resolution structural characterization. The only structured part appears to be the tetramerization domain, which has been investigated by bioinformatic tools (26), resistance to protease digestion (28, 41), and deletion series (13, 25, 42). Although fragment Y*, which exhibits high stability and homogeneity (25, 27, 28), has been acknowledged as the core of the tetramerization domain, the OD of hRSV P is often represented by fragment X (Table 1), longer then Y* by 15 residues at its N terminus. Predicted structural models of fragment X present this stretch as a second short coiled-coil domain (28, 42). We show here that this stretch has no significant SSP and is highly dynamic in solution, at least in the absence of protein partners. This is also in agreement with the observation that P_{ND} was not able to form oligomers (25).

In contrast to *Mononegavirales* N proteins, which share a conserved fold (43), P proteins have largely diverged, hRSV P having the shortest sequence (44). However, several regions of P are highly conserved among *Pneumoviridae*, more particularly the OD (Fig. 6*A*). Its structure was solved by X-ray diffraction for hMPV P (45). It displays a coiled-coil helical conformation for a region equivalent to the hRSV fragment Y*, indicating that a short OD is specific of this family. The protomers are arranged in a parallel orientation, consistently with the PRE

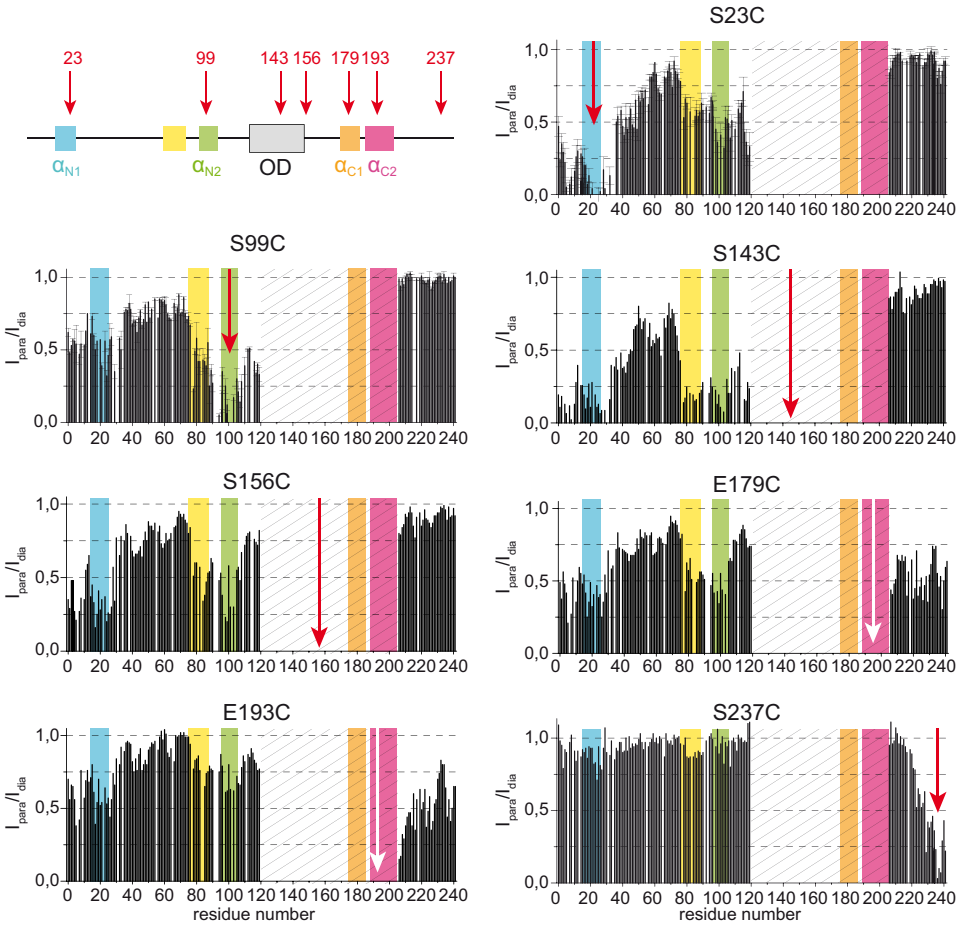

FIGURE 3. **Evidence for long-range contacts in hRSV P by paramagnetic relaxation enhancement.** PREs were measured with nitroxide spin labels at positions 23, 99, 143, 156, 179, 193, and 237 in the sequence of P. *Hatched* areas indicate regions with missing amide signal in the diamagnetic state. *Error bars* represent the root mean square deviations calculated from two data sets. The position of the spin label is indicated by an *arrow* on each bar diagram. Transient secondary structure elements are indicated by colored background.

results for hRSV P, and not as a dimer of anti-parallel dimers like in Mumps virus P (46, 47).

Finally, we were able to identify a C-terminal domain with high α-helical propensity, whose dynamics are distinct from those of the OD and the fully disordered C terminus. The presence of transient C-terminal helices was also proposed for hMPV, based on small angle X-ray scattering data (45), showing that they constitute another hallmark of *Pneumoviridae*. But whereas α_{C1} is partly conserved, α_{C2} appears to be specific of the *Orthopneumovirus* genus (Fig. 6*A*). A tentative structural model of P in its most disordered state, summarizing the structural information determined by NMR, is given in Fig. 6*B*.

Functional Relevance of Transiently Structured Regions in hRSV P—The central role of the phosphoprotein in hRSV replication is associated to its role as a hub inside the RdRp complex, mediating interactions with both viral and cellular proteins (18, 24, 48). We show here that two regions identified before as binding regions for N^{mono} (24) and M2-1 (17, 18), α_{N1} and α_{N2}, respectively, display weak α-helical propensity. These transient helices might fold completely upon binding, as related for other protein-protein interactions (36, 37). Such a hypothesis would be supported by the large number (~30) of N-terminal P residues involved in the interaction with N^{mono} (Fig. 4). Our definition of α_{N1} matches with the second helix formed by hMPV P_{1-28} in the X-ray structure of the N^0·P complex (40). The sequence of α_{N1} is rather well conserved among *Pneumoviridae* (Fig. 6*A*), suggesting that α_{N1} constitutes a molecular recognition element for N^0.

Contradictory data are available for the interaction properties of the α-helical C-terminal domain of P. Immunoprecipitation assays showed that deletion of residues 160–180 impaired N binding in bRSV P (49), but not in hRSV P (50), despite high sequence conservation of N and P between hRSV and bRSV. This internal region partly overlaps with α_{C1} and was also perturbed in NMR interaction experiments with N_{NTD} (Fig. 4), which prompted us to propose it as a secondary N binding site. Moreover, temperature-sensitive mutations of P were reported in the same region (50). G172S and E176G do not support replication at 37 °C, which was linked to decreased interaction between N and P. The triple mutant R174A/E175A/E176A proved non-functional in a minigenome assay, but was still able to bind to N. Finally, a recombinant E176G RSV virus reverted to Asp^{176} (50). These data underline the functional importance of residue Glu^{176}, which contributes to a negative cluster with Glu^{175} and Glu^{179}, exacerbated in the structural context of the α_{C1} helix (Fig. 6*B*). If we link these results with the lability of α_{C1}, it appears that structural modulation of this helix could have a direct impact on RSV replication. In contrast,

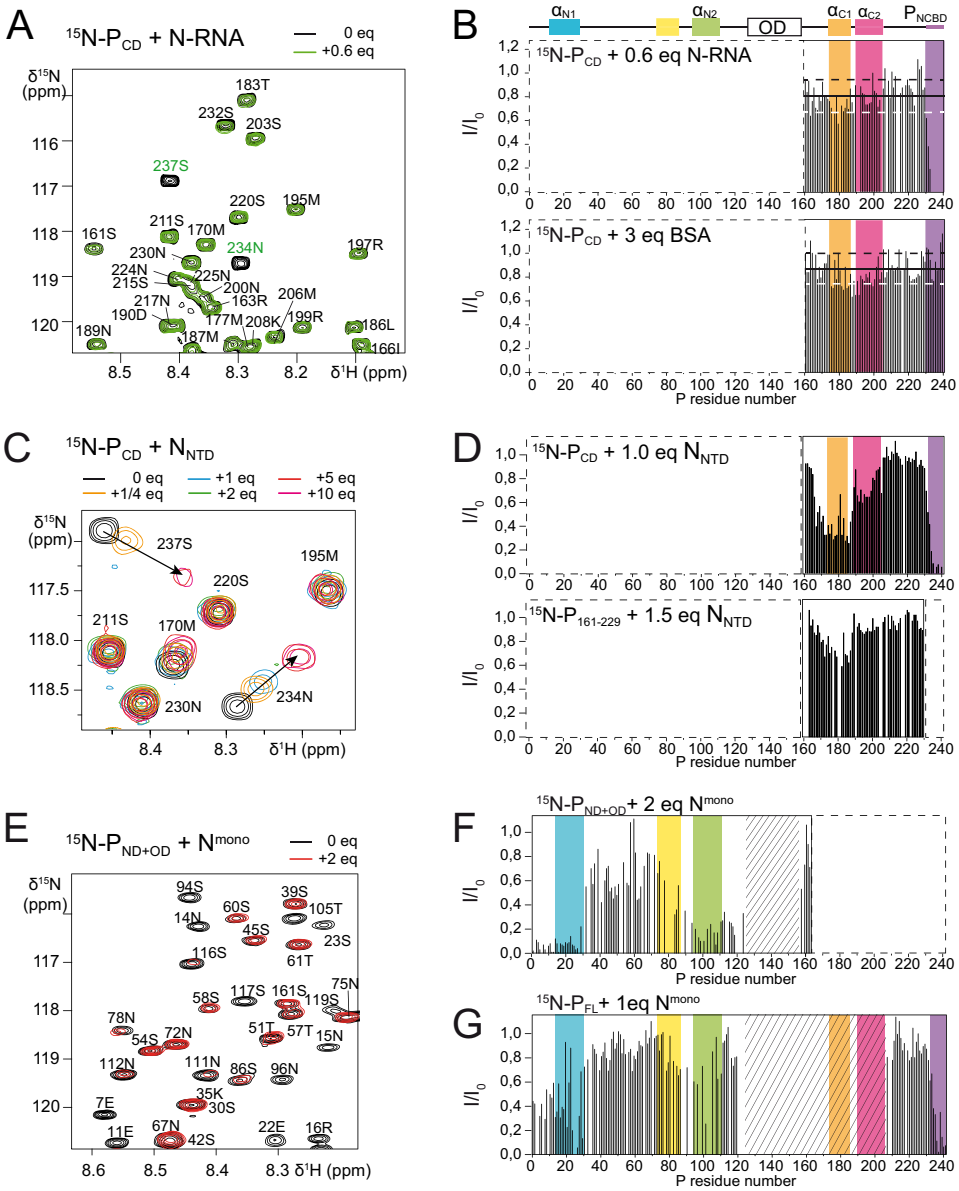

FIGURE 4. **Probing N/P interactions by NMR using ^{15}N-labeled P constructs.** *A,* selected region of the ^{1}H-^{15}N HSQC spectrum of ^{15}N-P_{CD} before and after addition of N-RNA rings. *B,* intensity ratios (I/I_0) for ^{15}N-P_{CD} in the presence of N-RNA rings measured from the ^{1}H-^{15}N HSQC spectra shown in *A*. A control experiment was carried out with 3 eq of BSA. Mean ± S.D. are indicated with *full* and *broken horizontal lines,* respectively. Background colors indicate transient secondary structure elements and the nucleocapsid binding domain (P_{NCBD}). *C,* titration of ^{15}N-P_{CD} by N_{NTD} followed by chemical shift and intensity variations. *D,* intensity ratios measured for ^{15}N-P_{CD} and ^{15}N-$P_{161–229}$ in the presence of N_{NTD}. *E,* selected region of the ^{1}H-^{15}N HSQC spectrum of ^{15}N-P_{ND+OD} before and after addition of N^{mono}. *F,* intensity ratios for ^{15}N-P_{ND+OD} in the presence of N^{mono} measured from *E*. The *hatched area* indicates missing amide signals for free P_{ND+OD}. *G,* intensity ratios measured for ^{15}N-P_{FL} in the presence of N^{mono}.

Leu^{198}-Asn^{217} has been reported to be a "negative N-binding region," the deletion of which enhanced N binding (16). This region partly overlaps with α_{C2} and was not affected by N_{NTD} in our experiments (Fig. 4).

Disordered Regions in hRSV P Mediate Diffuse as Well as Specific Interactions—In light of the X-ray structure of the hMPV N^0·P complex (40), the hRSV P_{40}/N_{NTD} interaction does not seem to be relevant for the N^0·P complex. However, it may shed light on the binding properties of α_{N1}. The interaction surfaces on N_{NTD} and N^0 are proximal and connected by the interaction surface with the N-terminal arm of an adjacent protomer in N-RNA rings (Fig. 5*E*). The P_{40}/N_{NTD} interaction might therefore correspond to an intermediate state on the binding/folding pathway of α_{N1}, whereby hydrophobic interactions play a role, as shown by the hydrophobic face in fully formed α_{N1} (Fig. 6*B*), involved in N^0 binding (40). α_{N1} appears to be a sticky helix that is able to mediate external (N/P) as well as internal interactions, the latter being favored by the tetrameric organization of P.

More generally, we identified transient internal long-range contacts in hRSV by PRE, mainly mediated by regions with SSPs. These seemingly unspecific interactions may play several roles. Compaction of the structure of P can be achieved, preventing unspecific interactions with other proteins in the cell. The interplay between α_{N1} and α_{N2}, which both expose hydrophobic faces when stabilized (Fig. 6*B*), suggests that upon bind-

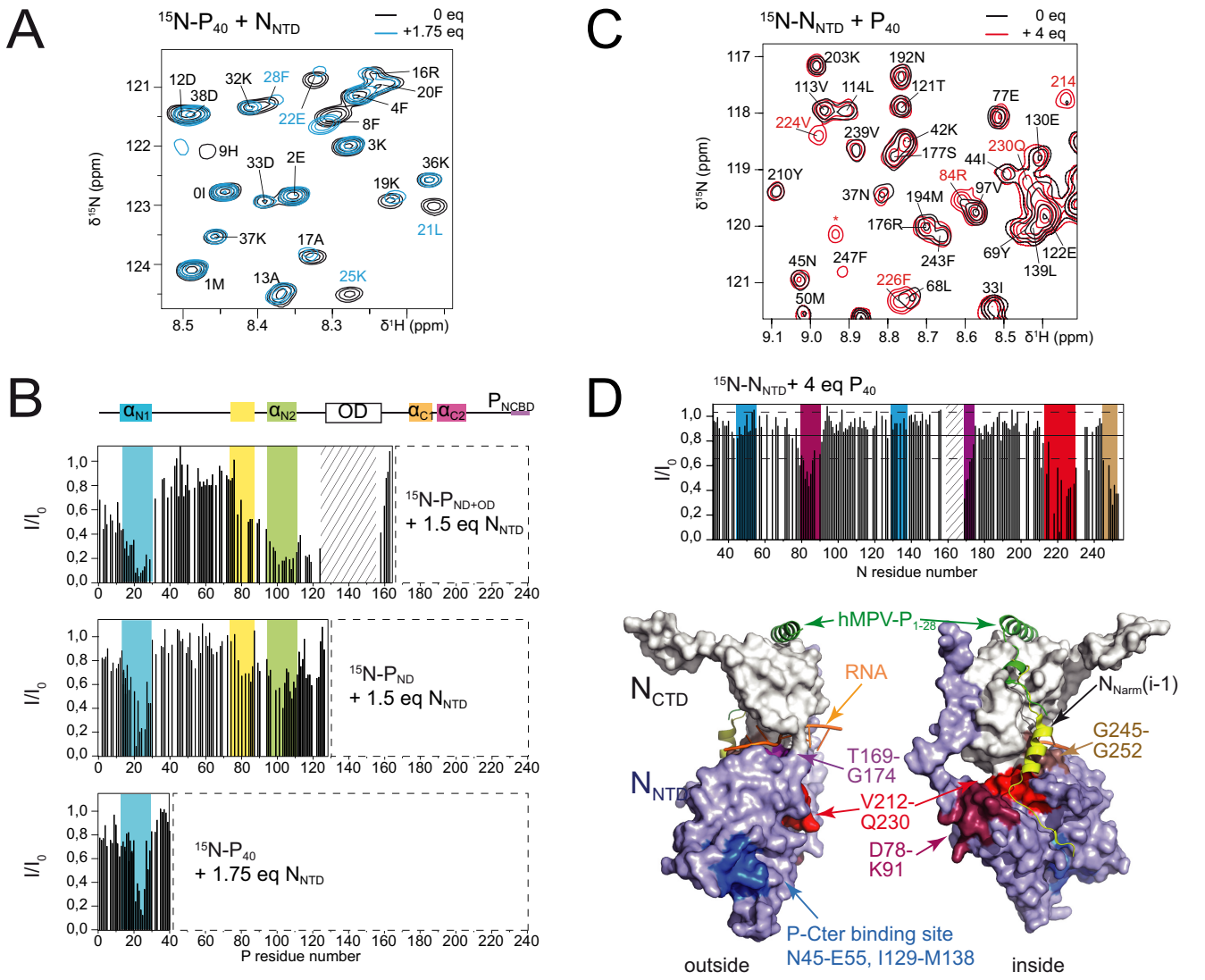

FIGURE 5. **Interaction between hRSV N_{NTD} and the N terminus of P.** *A*, selected region of the ^{1}H-^{15}N HSQC spectrum of ^{15}N-P_{40} in the presence or absence of N_{NTD}. *B*, intensity ratios (I/I_0) measured from ^{1}H-^{15}N HSQC spectra of ^{15}N-labeled N-terminal fragments of P in the presence of N_{NTD}. The *hatched* area indicates missing signals in the free forms. The background is colored according to transient secondary structures as indicated above. *C*, selected region of the ^{1}H-^{15}N HSQC spectrum of ^{15}N-N_{NTD} in the presence or absence of P_{40}. *D*, intensity ratios for ^{15}N-N_{NTD} in the presence of P_{40} measured from *C*. *Full* and *broken horizontal lines* indicate the mean ± S.D., respectively. Regions with significant line broadening (I/I_0 < mean −1 S.D.) are highlighted by *red to brown* backgrounds and the P C terminus binding region by *blue* color (39). The *hatched* area corresponds to unassigned N_{NTD} residues Ile^{160}-Val^{167}. The same color code is used to map these regions on the three-dimensional structure of an N protomer of N-RNA rings (PDB 2WJ8). The two views in surface representation are rotated by 180° and show the outside and inside of the N-RNA ring. The N-terminal arm (Ala^{2}-Gly^{30}) of the preceding N protomer in the ring (i-1) is in *yellow* schematic. The N-terminal P_{1-28} peptide of the hMPV N^{0}-P complex (PDB 5FVD) (40) in *green* schematic was superimposed onto hRSV N.

ing to one site, another site could become competent for binding. Plasticity of the structure of P can also help fulfilling the requirement of simultaneous binding at the C and N terminus to a same protein partner, *e.g.* to N. At the same time diffuse interactions may play a role by retaining RdRp relevant proteins in hRSV inclusion bodies (8).

The hRSV L binding site was recently reported to span residues Pro^{218}-Glu^{239} (Fig. 6*B*), and it was proposed that this region might fold into a helix (30). Under our experimental conditions this region did not display any significant SSP, conformational exchange, or internal contacts, similarly to P_{NCBD}. Analogy with P_{NCBD} suggests that this region might not fold upon binding. Except for Phe^{241}, P_{NCBD} is disordered in its bound form, as shown by X-ray crystal structures of N_{NTD} complexed to C-terminal P peptides (39). Although Phe^{241} is essential for NC·P binding, fuzzy electrostatic interactions mediated by acidic residues as well as phosphorylation of serines in P_{NCBD} significantly contribute to the affinity of P (14, 39, 51). Our NMR data suggest that even Phe^{241}, the linchpin for P binding to the NC, could explore different binding sites. Interactions that come into play in the NC·P complex are thus based on disorder and on a balance between recognition and moderate affinity, required for the processivity of the polymerase. This could be a more general scheme for P interactions with other RdRp components.

Experimental Procedures

Plasmids—Plasmids for expression of recombinant hRSV proteins in *E. coli* were described previously for N terminally GST-fused hRSV phosphoprotein and P fragments listed in

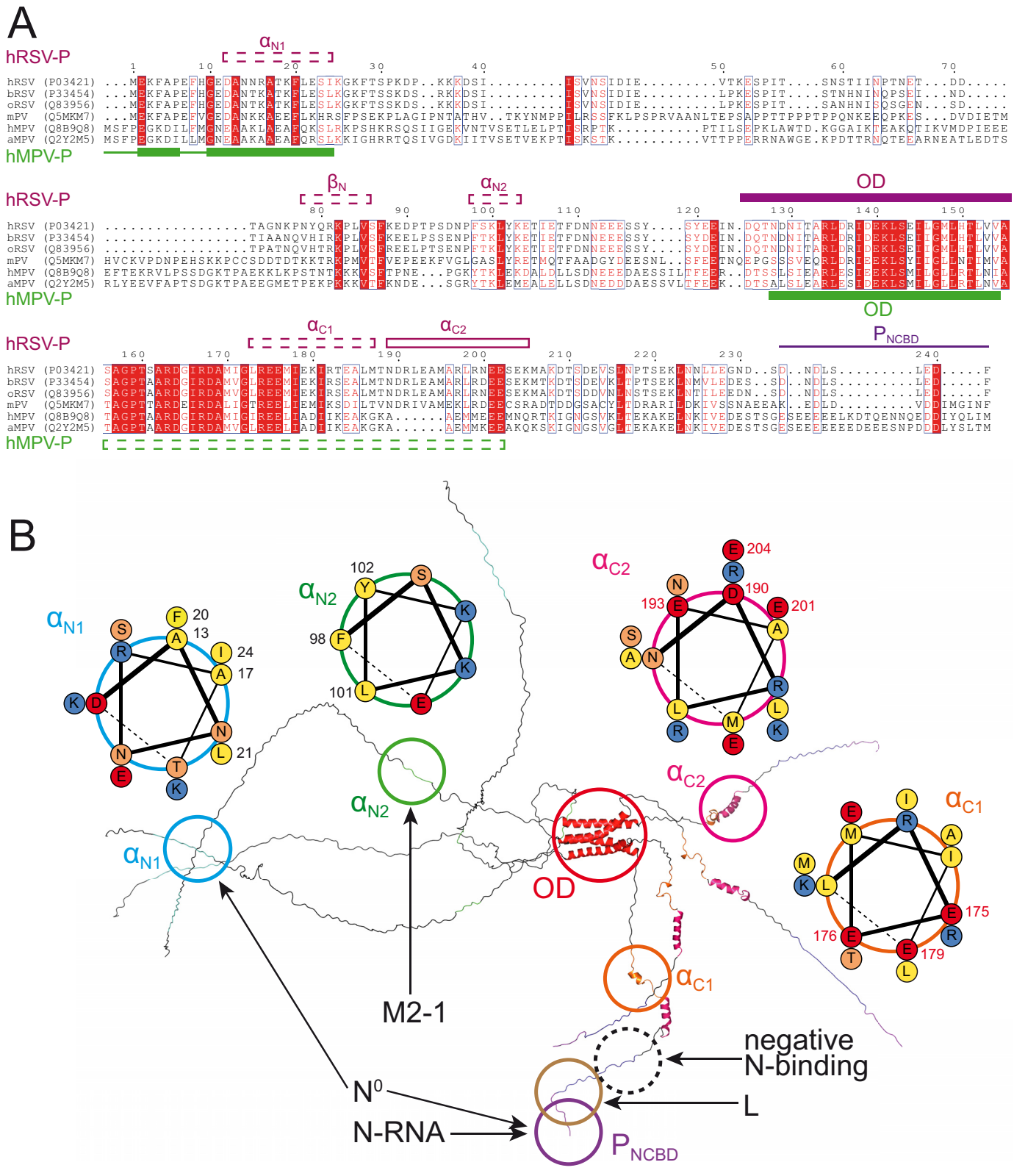

FIGURE 6. **Location of structural elements and binding sites in hRSV P.** *A,* sequence alignment of *Pneumoviridae* phosphoproteins for human, bovine, and ovine respiratory syncytial virus, murine pneumonia virus, human and avian metapneumovirus, generated with Clustal Omega (57) and displayed with ESPript (58). Uniprot accession numbers are shown in *parentheses*. On *top* are indicated hRSV P secondary structure elements determined by NMR, with almost stable and transient elements in *full* and *broken lines*, respectively. At the *bottom* are indicated known secondary structure elements for hMPV P (40, 45). *B,* structural model of the hRSV P tetramer. The location of regions with α-helical propensity is shown and their sequences are given in helical wheel representation. The location of RdRp protein binding sites is also shown, for regions with and without significant SSPs.

Table 1 (13, 24, 25, 30) and C terminally His-tagged hRSV nucleoprotein (13), N_{NTD} (N residues 31–252) (14), and the K170A/R185A N^{mono} mutant (24).

Expression and Purification of Proteins—All proteins were expressed in *E. coli* BL21(DE3). ^{15}N- and ^{15}N,^{13}C-labeled P protein samples for NMR experiments were produced in minimum M9 medium supplemented with 1 g liter^{-1} $^{15}NH_4Cl$ (Eurisotop), 4 or 3 g liter^{-1} unlabeled or ^{13}C-labeled glucose (Eurisotop), and 100 μg ml^{-1} of ampicillin, using a protocol adapted from cultures in rich medium (30). Bacteria were disrupted (Constant Systems Ltd) in 50 mM Tris, pH 7.8, 60 mM NaCl, 1 mM EDTA, 2 mM β-mercaptoethanol, 0.2% Triton X-100 lysis buffer. After clarification by ultracentrifugation the supernatant was mixed with 2 ml of glutathione-Sepharose beads (GE Healthcare) per liter of culture and incubated for 15 h at 4 °C. The resin beads were then washed with thrombin cleavage buffer (20 mM Tris, pH 8.4, 150 mM NaCl, 2 mM β-mercaptoethanol, 2.5 mM $CaCl_2$) before addition of 5 units of biotinylated thrombin (Novagen). The beads were incubated for 16 h at 4 °C. Thrombin was removed with streptavidin resin (Novagen) according to the manufacturer's instructions. Purification of N protein was carried out as described previously for N^{mono} (24), N_{NTD} (39), and N-RNA rings (13). His tags were not removed. The quality of protein samples was assessed by SDS-PAGE. Samples were subsequently dialyzed into NMR buffer (20 mM sodium phosphate, pH 6.5, 100 mM NaCl) and concentrated to 50–300 μM on Amicon Ultra centrifugal filters (10 kDa cut-off, Merck-Millipore).

Paramagnetic Spin Labeling—Individual residues of hRSV P, preferentially serines (Ser^{23}, Ser^{99}, Ser^{143}, Ser^{156}, Glu^{179}, Glu^{193}, Ser^{237}), were mutated into cysteines using the QuikChange mutagenesis kit (Stratagene). Mutant proteins were expressed and purified like wild type. Buffers contained 5 mM dithiothreitol (DTT) as a reducing agent. Protein samples were completely reduced by addition of another 5 mM DTT at room temperature for 2 h. DTT was then removed by passing twice through a Biospin desalting column (Bio-Rad) equilibrated in 50 mM Tris, pH 8.0, 200 mM NaCl. Protein samples were reacted overnight in the dark at 15 °C with 10 molar eq of 3-(2-iodoacetamido)-PROXYL radical (IAP, Sigma) in a 45 mM solution in ethanol. Unreacted IAP was removed by applying the samples three times onto Biospin desalting columns equilibrated in NMR buffer.

NMR Spectroscopy—NMR measurements were carried out on a Bruker Avance III spectrometer at a magnetic field of 14.1 T (600 MHz ^{1}H frequency) equipped with a cryogenic TCI probe. The magnetic field was locked with 7% ^2H_2O. The temperature was 288 K if not indicated otherwise. Spectra were processed with Topspin 3.1 (Bruker Biospin) and analyzed with CCPNMR 2.2 (52).

Sequential backbone assignment of the hRSV phosphoprotein constructs was carried out with BEST versions of HNCA, HN(CO)CA, HNCACB, HN(CO)CACB, and HNCO triple resonance experiments (53). $^1H\alpha$ chemical shifts were obtained from HNHA or HBHA(CO)NH experiments. ^{1}H and ^{13}C chemical shifts were referenced to 4,4-dimethyl-4-silapentane-1-sulfonic acid. Assignment completeness was 95% amides, 87% $^{13}C'$, 98% $^{13}C\alpha$, 60% $^{13}C\beta$, and 86% $^1H\alpha$ for P_{ND}; 74% amides, 69% $^{13}C'$, 79% $^{13}C\alpha$, 79% $^{13}C\beta$, and 76% $^1H\alpha$ for P_{ND+OD}; 98% amides, 95% $^{13}C'$, 98% $^{13}C\alpha$, 99% $^{13}C\beta$, and 93% $^1H\alpha$ for P_{CD}; 95% amides, 93% $^{13}C'$, 99% $^{13}C\alpha$, 99% $^{13}C\beta$, 81% $^1H\alpha$, and 78% $^1H\beta$ for $P_{\Delta OD}$; 61% amides, 59% $^{13}C'$, 64% $^{13}C\alpha$, 64% $^{13}C\beta$, 56% $^1H\alpha$, and 57% $^1H\beta$ for P_{FL} (S23C mutant).

NMR Interaction Experiments—NMR interaction experiments were carried out at a magnetic field of 14.1 T by acquiring ^{1}H-^{15}N HSQC spectra of ^{15}N-labeled P constructs in a 30–100 μM concentration range in the presence of 0.25 to 10 molar eq of unlabeled N protein in the form of N_{NTD}, N^{mono}, or N-RNA rings. Samples were prepared by mixing concentrated protein solutions. Line broadening was analyzed by measuring the intensity ratios of amide signals between the spectra with and without N protein in CCPNMR 2.2. Dissociation constants for the P_{CD}·N_{NTD} complex were determined for each perturbed residue by assuming a two-site fast exchange model with a 1:1 stoichiometry and by fitting ^{1}H and ^{15}N chemical shift differences with Origin 7 (OriginLab) according to Equation 1,

$$(\delta - \delta_{free}) = \frac{1}{2}(\delta_{bound} - \delta_{free})(A + r - \sqrt{(A + r)^2 - 4r}) \quad \text{(Eq. 1)}$$

where $r = [N]_{tot}/[P_{CD}]_{tot}$, $K_d = (A - 1) \times [P_{CD}]_{tot}$ and $[P_{CD}]_{tot} = 50\ \mu$M.

Complementary experiments were performed with ^{15}N-N_{NTD} (50 μM in 20 mM MES, pH 6.5, 250 mM NaCl buffer) at 293 K, by adding lyophilized P_{40} with 1:1 to 12:1 ratios (solubility limit).

^{15}N Relaxation Measurements—^{15}N relaxation data were recorded at a magnetic field of 14.1 T and a temperature of 288 K. R_1 and R_2 relaxation rates were measured for 50–200 μM ^{15}N-labeled P_{ND}, P_{ND+OD}, P_{CD}, and $P_{\Delta OD}$ with a pseudo-three-dimensional version recorded in an interleaved manner with a recycling delay of 4 s. Relaxation delays were 5, 50, 100, 200(*2), 400, 600, 800, 1200, and 2000 ms for R_1 measurements and 34, 68, 136, 204(*2), 271, 339, 407, 543, and 814 ms for R_2. Heteronuclear ^{1}H-^{15}N NOEs were measured by recording two interleaved spectra with on- and off-resonance ^{1}H saturation during the recycling delay. Peak intensities were extracted in CCPNMR 2.2. Relaxation curves were fitted to a monoexponential model and errors estimated from covariance matrix analysis in CCPNMR 2.2.

PRE Measurements—PREs were determined as the ratios between ^{1}H-^{15}N HSQC peak intensities in the paramagnetic and diamagnetic state (I_{para}/I_{dia}). Measurements were carried out at 14.1 T and 288 K. The diamagnetic state was obtained by incubating the spin-labeled sample with 10 molar eq of ascorbic acid (Sigma) from a 45 mM solution at pH 6.5 for 3–4 h at 303 K.

Modeling—Homology modeling of OD residues Asp^{129}-Leu^{152} was done with Modeler 9v16 (54) using hMPV Leu^{170}-Leu^{193} (PDB 4BXT) as a template. P IDRs were built in CYANA 3.97 (55) by using dihedral angle restraints generated from P_{CD} backbone chemical shifts with Talos+ (31).

Illustrations—Figures were prepared using PyMOL (56). Helical wheel diagrams were generated with DrawCoil 1.0.

Author Contributions—C. S. conceived and coordinated the study and wrote the paper. E. L., F. B., J. F. E., M. G., and N. A. participated in early experiments and provided assistance in sample preparation or NMR spectroscopy. C. C., C. S., J. F., M. G., N. P., and S. L. conducted and analyzed experiments. All authors reviewed the results and approved the final version of the manuscript.

References

1. Afonso, C. L., Amarasinghe, G. K., Banyai, K., Bao, Y., Basler, C. F., Bavari, S., Bejerman, N., Blasdell, K. R., Briand, F. X., Briese, T., Bukreyev, A., Calisher, C. H., Chandran, K., Cheng, J., Clawson, A. N., *et al*. (2016) Taxonomy of the order mononegavirales: update 2016. *Arch. Virol.* **161,** 2351–2360
2. Collins, P. L., and Melero, J. A. (2011) Progress in understanding and controlling respiratory syncytial virus: still crazy after all these years. *Virus Res.* **162,** 80–99
3. Nair, H., Nokes, D. J., Gessner, B. D., Dherani, M., Madhi, S. A., Singleton, R. J., O'Brien, K. L., Roca, A., Wright, P. F., Bruce, N., Chandran, A., Theodoratou, E., Sutanto, A., Sedyaningsih, E. R., Ngama, M., *et al*. (2010) Global burden of acute lower respiratory infections due to respiratory syncytial virus in young children: a systematic review and meta-analysis. *Lancet* **375,** 1545–1555
4. Mazur, N. I., Martinón-Torres, F., Baraldi, E., Fauroux, B., Greenough, A., Heikkinen, T., Manzoni, P., Mejias, A., Nair, H., Papadopoulos, N. G., Polack, F. P., Ramilo, O., Sharland, M., Stein, R., Madhi, S. A., Bont, L., and Respiratory Syncytial Virus Network (ReSViNET) (2015) Lower respiratory tract infection caused by respiratory syncytial virus: current management and new therapeutics. *Lancet Respir. Med.* **3,** 888–900
5. Collins, P. L., and Karron, R. A. (2013) Respiratory Syncytial Virus and Metapneumovirus. in *Fields Virology* (Knipe, D. M., and Howley, P. M., eds) 6th Ed., pp. 1086–1123, Lippinscot Williams & Wilkins, Wolters Kluwer, Philadelphia, PA
6. Cox, R., and Plemper, R. K. (2016) Structure-guided design of small-molecule therapeutics against RSV disease. *Expert Opin. Drug Discov.* **11,** 543–556
7. Cox, R., and Plemper, R. K. (2015) The paramyxovirus polymerase complex as a target for next-generation anti-paramyxovirus therapeutics. *Front. Microbiol.* **6,** 459
8. García, J., García-Barreno, B., Vivo, A., and Melero, J. A. (1993) Cytoplasmic inclusions of respiratory syncytial virus-infected cells: formation of inclusion bodies in transfected cells that coexpress the nucleoprotein, the phosphoprotein, and the 22K protein. *Virology* **195,** 243–247
9. Lahaye, X., Vidy, A., Pomier, C., Obiang, L., Harper, F., Gaudin, Y., and Blondel, D. (2009) Functional characterization of Negri bodies (NBs) in rabies virus-infected cells: evidence that NBs are sites of viral transcription and replication. *J. Virol.* **83,** 7948–7958
10. Heinrich, B. S., Cureton, D. K., Rahmeh, A. A., and Whelan, S. P. (2010) Protein expression redirects vesicular stomatitis virus RNA synthesis to cytoplasmic inclusions. *PLoS Pathog.* **6,** e1000958
11. Grosfeld, H., Hill, M. G., and Collins, P. L. (1995) RNA replication by respiratory syncytial virus (RSV) is directed by the N, P, and L proteins; transcription also occurs under these conditions but requires RSV superinfection for efficient synthesis of full-length mRNA. *J. Virol.* **69,** 5677–5686
12. Yu, Q., Hardy, R. W., and Wertz, G. W. (1995) Functional cDNA clones of the human respiratory syncytial (RS) virus N, P, and L proteins support replication of RS virus genomic RNA analogs and define minimal trans-acting requirements for RNA replication. *J. Virol.* **69,** 2412–2419
13. Tran, T. L., Castagné, N., Bhella, D., Varela, P. F., Bernard, J., Chilmonczyk, S., Berkenkamp, S., Benhamo, V., Grznarova, K., Grosclaude, J., Nespoulos, C., Rey, F. A., and Eléouët, J. F. (2007) The nine C-terminal amino acids of the respiratory syncytial virus protein P are necessary and sufficient for binding to ribonucleoprotein complexes in which six ribonucleotides are contacted per N protein protomer. *J. Gen. Virol.* **88,** 196–206
14. Galloux, M., Tarus, B., Blazevic, I., Fix, J., Duquerroy, S., and Eléouët, J. F. (2012) Characterization of a viral phosphoprotein binding site on the surface of the respiratory syncytial nucleoprotein. *J. Virol.* **86,** 8375–8387
15. García-Barreno, B., Delgado, T., and Melero, J. A. (1996) Identification of protein regions involved in the interaction of human respiratory syncytial virus phosphoprotein and nucleoprotein: significance for nucleocapsid assembly and formation of cytoplasmic inclusions. *J. Virol.* **70,** 801–808
16. Slack, M. S., and Easton, A. J. (1998) Characterization of the interaction of the human respiratory syncytial virus phosphoprotein and nucleocapsid protein using the two-hybrid system. *Virus Res.* **55,** 167–176
17. Mason, S. W., Aberg, E., Lawetz, C., DeLong, R., Whitehead, P., and Liuzzi, M. (2003) Interaction between human respiratory syncytial virus (RSV) M2-1 and P proteins is required for reconstitution of M2-1-dependent RSV minigenome activity. *J. Virol.* **77,** 10670–10676
18. Blondot, M. L., Dubosclard, V., Fix, J., Lassoued, S., Aumont-Nicaise, M., Bontems, F., Eléouët, J. F., and Sizun, C. (2012) Structure and functional analysis of the RNA- and viral phosphoprotein-binding domain of respiratory syncytial virus M2–1 protein. *PLoS Pathog.* **8,** e1002734
19. Tran, T. L., Castagné, N., Dubosclard, V., Noinville, S., Koch, E., Moudjou, M., Henry, C., Bernard, J., Yeo, R. P., and Eléouët, J. F. (2009) The respiratory syncytial virus M2-1 protein forms tetramers and interacts with RNA and P in a competitive manner. *J. Virol.* **83,** 6363–6374
20. Villanueva, N., Hardy, R., Asenjo, A., Yu, Q., and Wertz, G. (2000) The bulk of the phosphorylation of human respiratory syncytial virus phosphoprotein is not essential but modulates viral RNA transcription and replication. *J. Gen. Virol.* **81,** 129–133
21. Asenjo, A., Calvo, E., and Villanueva, N. (2006) Phosphorylation of human respiratory syncytial virus P protein at threonine 108 controls its interaction with the M2-1 protein in the viral RNA polymerase complex. *J. Gen. Virol.* **87,** 3637–3642
22. Asenjo, A., and Villanueva, N. (2016) Phosphorylation of the human respiratory syncytial virus P protein mediates M2-2 regulation of viral RNA synthesis, a process that involves two P proteins. *Virus Res.* **211,** 117–125
23. Curran, J., Marq, J. B., and Kolakofsky, D. (1995) An N-terminal domain of the Sendai paramyxovirus P protein acts as a chaperone for the NP protein during the nascent chain assembly step of genome replication. *J. Virol.* **69,** 849–855
24. Galloux, M., Gabiane, G., Sourimant, J., Richard, C. A., England, P., Moudjou, M., Aumont-Nicaise, M., Fix, J., Rameix-Welti, M. A., and Eléouët, J. F. (2015) Identification and characterization of the binding site of the respiratory syncytial virus phosphoprotein to RNA-free nucleoprotein. *J. Virol.* **89,** 3484–3496
25. Castagné, N., Barbier, A., Bernard, J., Rezaei, H., Huet, J. C., Henry, C., Da Costa, B., and Eléouët, J. F. (2004) Biochemical characterization of the respiratory syncytial virus P-P and P-N protein complexes and localization of the P protein oligomerization domain. *J. Gen. Virol.* **85,** 1643–1653
26. Simabuco, F. M., Asara, J. M., Guerrero, M. C., Libermann, T. A., Zerbini, L. F., and Ventura, A. M. (2011) Structural analysis of human respiratory syncytial virus p protein: identification of intrinsically disordered domains. *Braz. J. Microbiol.* **42,** 340–345
27. Noval, M. G., Esperante, S. A., Molina, I. G., Chemes, L. B., and Prat-Gay, G. (2016) Intrinsic disorder to order transitions in the scaffold phosphoprotein P from the respiratory syncytial virus RNA polymerase complex. *Biochemistry* **55,** 1441–1454
28. Llorente, M. T., Taylor, I. A., López-Viñas, E., Gomez-Puertas, P., Calder, L. J., García-Barreno, B., and Melero, J. A. (2008) Structural properties of the human respiratory syncytial virus P protein: evidence for an elongated homotetrameric molecule that is the smallest orthologue within the family of paramyxovirus polymerase cofactors. *Proteins* **72,** 946–958
29. Kosol, S., Contreras-Martos, S., Cedeño, C., and Tompa, P. (2013) Structural characterization of intrinsically disordered proteins by NMR spectroscopy. *Molecules* **18,** 10802–10828
30. Sourimant, J., Rameix-Welti, M. A., Gaillard, A. L., Chevret, D., Galloux, M., Gault, E., and Eléouët, J. F. (2015) Fine mapping and characterization of the L-polymerase-binding domain of the respiratory syncytial virus phosphoprotein. *J. Virol.* **89,** 4421–4433

31. Shen, Y., Delaglio, F., Cornilescu, G., and Bax, A. (2009) TALOS+: a hybrid method for predicting protein backbone torsion angles from NMR chemical shifts. *J. Biomol. NMR* **44,** 213–223
32. Camilloni, C., De Simone, A., Vranken, W. F., and Vendruscolo, M. (2012) Determination of secondary structure populations in disordered states of proteins using nuclear magnetic resonance chemical shifts. *Biochemistry* **51,** 2224–2231
33. Clore, G. M., and Iwahara, J. (2009) Theory, practice, and applications of paramagnetic relaxation enhancement for the characterization of transient low-population states of biological macromolecules and their complexes. *Chem. Rev.* **109,** 4108–4139
34. Lietzow, M. A., Jamin, M., Dyson, H. J., and Wright, P. E. (2002) Mapping long-range contacts in a highly unfolded protein. *J. Mol. Biol.* **322,** 655–662
35. Gillespie, J. R., and Shortle, D. (1997) Characterization of long-range structure in the denatured state of staphylococcal nuclease: I. paramagnetic relaxation enhancement by nitroxide spin labels. *J. Mol. Biol.* **268,** 158–169
36. Wright, P. E., and Dyson, H. J. (2009) Linking folding and binding. *Curr. Opin. Struct. Biol.* **19,** 31–38
37. Mohan, A., Oldfield, C. J., Radivojac, P., Vacic, V., Cortese, M. S., Dunker, A. K., and Uversky, V. N. (2006) Analysis of molecular recognition features (MoRFs). *J. Mol. Biol.* **362,** 1043–1059
38. Bakker, S. E., Duquerroy, S., Galloux, M., Loney, C., Conner, E., Eléouët, J. F., Rey, F. A., and Bhella, D. (2013) The respiratory syncytial virus nucleoprotein-RNA complex forms a left-handed helical nucleocapsid. *J. Gen. Virol.* **94,** 1734–1738
39. Ouizougun-Oubari, M., Pereira, N., Tarus, B., Galloux, M., Lassoued, S., Fix, J., Tortorici, M. A., Hoos, S., Baron, B., England, P., Desmaele, D., Couvreur, P., Bontems, F., Rey, F. A., *et al*. (2015) A druggable pocket at the nucleocapsid/phosphoprotein interaction site of human respiratory syncytial virus. *J. Virol.* **89,** 11129–11143
40. Renner, M., Bertinelli, M., Leyrat, C., Paesen, G. C., Saraiva de Oliveira, L. F., Huiskonen, J. T., and Grimes, J. M. (2016) Nucleocapsid assembly in pneumoviruses is regulated by conformational switching of the N protein. *Elife* **5,** e12627
41. Llorente, M. T., García-Barreno, B., Calero, M., Camafeita, E., López, J. A., Longhi, S., Ferrón, F., Varela, P. F., and Melero, J. A. (2006) Structural analysis of the human respiratory syncytial virus phosphoprotein: characterization of an α-helical domain involved in oligomerization. *J. Gen. Virol.* **87,** 159–169
42. Asenjo, A., Mendieta, J., Gómez-Puertas, P., and Villanueva, N. (2008) Residues in human respiratory syncytial virus P protein that are essential for its activity on RNA viral synthesis. *Virus Res.* **132,** 160–173
43. Ruigrok, R. W., Crépin, T., and Kolakofsky, D. (2011) Nucleoproteins and nucleocapsids of negative-strand RNA viruses. *Curr. Opin. Microbiol.* **14,** 504–510
44. Karlin, D., and Belshaw, R. (2012) Detecting remote sequence homology in disordered proteins: discovery of conserved motifs in the N-termini of Mononegavirales phosphoproteins. *PLoS ONE* **7,** e31719
45. Leyrat, C., Renner, M., Harlos, K., and Grimes, J. M. (2013) Solution and crystallographic structures of the central region of the phosphoprotein from human metapneumovirus. *PLoS ONE* **8,** e80371
46. Cox, R., Green, T. J., Purushotham, S., Deivanayagam, C., Bedwell, G. J., Prevelige, P. E., and Luo, M. (2013) Structural and functional characterization of the mumps virus phosphoprotein. *J. Virol.* **87,** 7558–7568
47. Cox, R., Pickar, A., Qiu, S., Tsao, J., Rodenburg, C., Dokland, T., Elson, A., He, B., and Luo, M. (2014) Structural studies on the authentic mumps virus nucleocapsid showing uncoiling by the phosphoprotein. *Proc. Natl. Acad. Sci. U.S.A.* **111,** 15208–15213
48. Munday, D. C., Wu, W., Smith, N., Fix, J., Noton, S. L., Galloux, M., Touzelet, O., Armstrong, S. D., Dawson, J. M., Aljabr, W., Easton, A. J., Rameix-Welti, M. A., de Oliveira, A. P., Simabuco, F. M., Ventura, A. M., *et al*. (2015) Interactome analysis of the human respiratory syncytial virus RNA polymerase complex identifies protein chaperones as important cofactors that promote L-protein stability and RNA synthesis. *J. Virol.* **89,** 917–930
49. Khattar, S. K., Yunus, A. S., and Samal, S. K. (2001) Mapping the domains on the phosphoprotein of bovine respiratory syncytial virus required for N-P and P-L interactions using a minigenome system. *J. Gen. Virol.* **82,** 775–779
50. Lu, B., Brazas, R., Ma, C. H., Kristoff, T., Cheng, X., and Jin, H. (2002) Identification of temperature-sensitive mutations in the phosphoprotein of respiratory syncytial virus that are likely involved in its interaction with the nucleoprotein. *J. Virol.* **76,** 2871–2880
51. Shapiro, A. B., Gao, N., O'Connell, N., Hu, J., Thresher, J., Gu, R. F., Overman, R., Hardern, I. M., and Sproat, G. G. (2014) Quantitative investigation of the affinity of human respiratory syncytial virus phosphoprotein C-terminus binding to nucleocapsid protein. *Virol. J.* **11,** 191
52. Vranken, W. F., Boucher, W., Stevens, T. J., Fogh, R. H., Pajon, A., Llinas, M., Ulrich, E. L., Markley, J. L., Ionides, J., and Laue, E. D. (2005) The CCPN data model for NMR spectroscopy: development of a software pipeline. *Proteins* **59,** 687–696
53. Lescop, E., Schanda, P., and Brutscher, B. (2007) A set of BEST triple-resonance experiments for time-optimized protein resonance assignment. *J. Magn. Reson.* **187,** 163–169
54. Sali, A., and Blundell, T. L. (1993) Comparative protein modelling by satisfaction of spatial restraints. *J. Mol. Biol.* **234,** 779–815
55. Guntert, P. (2004) Automated NMR structure calculation with CYANA. *Methods Mol. Biol*. **278,** 353–378
56. Schrodinger, L. (2010) *The AxPyMOL Molecular Graphics Plugin for Microsoft PowerPoint*, version 1.0, Schrödinger, LLC, New York
57. Sievers, F., Wilm, A., Dineen, D., Gibson, T. J., Karplus, K., Li, W., Lopez, R., McWilliam, H., Remmert, M., Söding, J., Thompson, J. D., and Higgins, D. G. (2011) Fast, scalable generation of high-quality protein multiple sequence alignments using Clustal Omega. *Mol. Syst. Biol.* **7,** 539
58. Gouet, P., Courcelle, E., Stuart, D. I., and Metoz, F. (1999) ESPript, analysis of multiple sequence alignments in PostScript. *Bioinformatics* **15,** 305–308

New Insights into Structural Disorder in Human Respiratory Syncytial Virus Phosphoprotein and Implications for Binding of Protein Partners

Nelson Pereira, Christophe Cardone, Safa Lassoued, Marie Galloux, Jenna Fix, Nadine Assrir, Ewen Lescop, François Bontems, Jean-François Eléouët and Christina Sizun

J. Biol. Chem. 2017, 292:2120-2131.
doi: 10.1074/jbc.M116.765958 originally published online December 28, 2016